RSC Advances

ROYAL SOCIETY OF CHEMISTRY

www.rsc.org/advances

Revised

Fabrication of poly(methyl methacrylate) /silica KIT-6 nanocomposites via in situ polymerization approach and their application for removal of Cu^{2+} from aqueous solution

Mohammad Dinari[*] [a], Gholamhossein Mohammadnezhad[*] [a], Roozbeh Soltani [a]

[a]*Department of Chemistry, Isfahan University of Technology, Isfahan, 84156-83111, Islamic Republic of Iran*

[*] Corresponding authors. Tel.; +98-31-3391-3270; FAX: +98-31-3391-2350.

E-mail address: dinari@cc.iut.ac.ir, mdinary@gmail.com. (M. Dinari).

E-mail address: mohammadnezhad@cc.iut.ac.ir; g_m1358@yahoo.com (G. Mohammadnezhad).

Abstract In this study, three types of novel mesoporous silica nanocomposites (called MSNCs) based on poly(methyl methacrylate) and modified mesoporous silica KIT-6 were prepared. The chemical, structural and textural properties of MSNCs were characterized by several methods including FT-IR spectroscopy, field-emission scanning electron microscopy (FE-SEM), transmission electron microscopy (TEM), X-ray diffraction (XRD) and thermogravimetric analysis (TGA). Experimental results showed that MSNCs have many active sites on their surface and this feature is a promising future for targeting application like adsorption. Accordingly, its application for adsorption of Cu(II) from aqueous solution was examined. Adsorption behavior of Cu(II) onto pure KIT-6, modified KIT-6(called m-KIT-6) and three types of MSNCs were investigated by kinetic and isotherm studies. It was observed that the adsorption equilibrium is short (15 and 30 min for m-KIT-6 and pure KIT-6, respectively and 60-90 min for MSNCs). Adsorption kinetic was educated by pseudo second order kinetic equation. Also the maximum adsorptive capacities of tree types of MSNCs were 79.14 %, 91.20 % and 81.72 %, respectively. And finally, the resulting adsorption isotherms of the MSNCs as well as pure KIT-6 and m-KIT-6 were found to have the best fit to the Langmuir isotherm model.

Keywords Nanoporous silica; Poly(methyl methacrylate); In situ polymerization; Transmission electron microscopy (TEM); Adsorption mechanism

1. Introduction

Based on IUPAC, porous materials according to the pore diameter classified into three main categories including micro-(<2 nm), meso- (2–50 nm) and macroporous (>50 nm).[1] In the past decade, order mesoporous materials like carbon and silica materials with two dimensional (2D) structures such as FDU, MCM and SBA have been utilized in the areas of energy storage, drug delivery and biology, catalysis and adsorption, sensing, and sample preparation applications.[2-7] These widespread applications of mesoporous materials as mentioned is because of their unique properties such as extremely large surface areas and large pore volumes, tunable micro-texture, functionalizabile surface and chemical stability for recyclability. Nowadays, one of the most widely used applications of mesoporous materials is their using in the nanocomposites (NCs) industry as nanofillers.[8] Hence, the global market of NCs containing nano-sized fillers materials has been expanding rapidly owing to their marvelous electronic, optical, mechanical and barrier properties in comparison to the virgin materials.[9] As the size of polymer molecules is much smaller than the mesopore size (2-50 nm), so the penetration of the polymer chain into the mesopore space during the preparation of NC is easily possible for leading to the formation of intimate composites.

KIT-6 with three-dimensional (3D) cubic *Ia3d* symmetric structure and porous networks, possess high specific surface area, large pore volume, high hydrothermal stability and large readily tunable pores with thick pore walls.[10-12] KIT-6 with 3D mesoporous structure has advantages over mesoporous materials having one-dimensional (1D) or tow-dimensional (2D) arrays of pores, mainly because mesoporous materials with 3D pore structure provide more adsorption sites for modification and functionalization and they are more resistant to pore blocking and so have a good mass transfer of the reactant molecules through the channels.[13] Interconnected silica supports also significantly enhance the surface activity of the support for modification and linking between support and polymer in order to prepare

nanocomposites. In previous studies the superiority of KIT-6 as cubic 3D mesoporous material has reported for instance in catalyst, gas adsorption and separation, sensing, electrodes and supercapacitors, as well as drug delivery and cancer therapy applications.[10, 14-20]

Poly(methyl methacrylate) (PMMA) has been widely utilized as a versatile polymer due to its unique advantages, such as excellent optical transparency, good solvent resistance, low density, low cost, chemical resistance, good flexibility, and good physic-mechanical properties. Because of these properties PMMA has been widely used in the medicine, optical and supercapacitors, automobile, hydrogen storage material and construction industries.[21-26] However, PMMA has some drawbacks including brittle texture, low thermal and mechanical stability and insufficient surface hardness. It has been reported that, addition of mesoporous materials such as mesoporous carbon or silica to the polymer matrix like PMMA results in an increase in the performance of the polymer and its thermal and mechanical behavior.[27, 28] Since mesoporous silica are difficult to disperse evenly in polymer matrix, because of aggregation, for homogeneous dispersion of inorganic moiety into polymer matrix, introduction of organic groups as coupling agent into mesoporous silica is a useful method.[29]

Presence of heavy metal ions in the environment such as water and soil is a significant concern because of their harmful effects.[30, 31] With the increasing demand for economic large-scale water treatment applications, the development of novel, low-cost, stable and efficient sorbent, therefore, is of great significance.[32, 33] Recently, polymer nanocomposites (NCs) have received more and more attention for the removal of heavy metal ions from the contaminated waste water.[34] Therefore, in this study; we attempted to use novel hybrids of polymer and mesoporous silica to separate heavy metal ions from aqueous solution. At first, several novel mesoporous silica nanocomposites (MSNCs) were prepared by *in situ* polymerization method. PMMA as a polymer matrix was selected due to its low cost, low

toxicity, chemical resistance and excellent chemical properties. Silica KIT-6 was chosen as inorganic filler because of its highly interconnected and interpenetrating systems of channels, accordingly, good accessibility for modification and compatibility with the polymers like PMMA. The m-KIT-6 was prepared through the reaction between 3-mercaptopropyl-trimethoxysilane with hydroxyl groups of the surface mesoporous KIT-6. Methyl methacrylate (MMA) monomer infiltrated into the pores of the 3D structure of m-KIT-6 and different MSNCs were synthesized by *in-situ* polymerization. The structure and morphology of the resulting hybrid compounds were characterized by different methods such as Fourier transform-infrared (FT-IR) spectroscopy, X-ray powder diffraction (XRD), thermogravimetry analysis (TGA), field emission-scanning electron microscopy (FE-SEM), and transmission electron microscopy (TEM). Then, the application of the MSNCs for adsorption of Cu(II) from aqueous solution was examined. The contact time as a significant parameter on the removal of Cu(II) ions and the adsorption mechanism was investigated.

2. Experimental

2.1. Materials

3-Mercaptopropyl-trimethoxysilane, copper(II) nitrate trihydrate [$Cu(NO_3)_2.3H_2O$], tetraethyl orthosilicate (TEOS), methacrylate (MMA), benzoyl peroxide (BP), HCl and NaOH were purchased from Merck Chemical Co. and used without further purification. Triblock copolymer Pluronic P123 (average Mn=5800, $(EO)_{20}(PO)_{70}(EO)_{20}$) was purchased from Aldrich Chemical Inc.

2.2. Instruments

FT-IR spectra of the polymers were recorded with a Jasco-680 (Japan) spectrometer from 400 to 4000 cm^{-1}, using KBr pellet technique by making 60 scans at 4 cm^{-1} resolution. The small angle powder XRD data was measured by an XRD (Bruker Nanostar U) with Cu K_α radiation (λ = 0.1542 nm) at 45 kV and 100 mA. The diffraction patterns were collected

between 2θ of 0.7^{o} and 8^{o} at a scanning rate of 0.05 ^{o}/min. The scanning speed was 0.02 ^{o}/s. TGA of the samples were carried out in a nitrogen atmosphere by heating rate of 20 °C/min from room temperature to 800 °C using the STA503 TA instrument. The morphology of the nanostructure materials was examined by FE-SEM (HITACHI, S-4160) and a TEM (Philips CM 120, Netherlands). For SEM preparation, the powdered sample was dispersed in H_2O, and then the sediment was dried at room temperature before gold coating. For TEM, the powders were dispersed in isopropanol and a drop of this suspension was put on a carbon coated nickel grid. The sono-chemichal reaction was carried out on a MISONIX ultrasonic liquid processor, XL-2000 SERIES (Raleigh, North Carolina, USA). Ultrasound was a wave of frequency 2.25 × 104 Hz and power of 100 W. The concentrations of the metal ions in the solution were measured by use of flame atomic absorption spectrophotometer (Perkin-Elmer 2380-Waltham).

2.3. Preparation of ordered mesoporous silica's, KIT-6

Mesoporous silica KIT-6 was prepared according to a previous report.[35] In a typical synthesis, 2.0 g of triblock copolymer P123 ($EO_{20}PO_{70}EO_{20}$) was dissolved in a solution with 7.0 g of HCl (36wt%) and 60.0 g of deionized water under stirring at room temperature. Then, 2.0 g of n-butanol was added to the solution and after 1h, 4.0 g of tetraethoxysilane was added. The mixture was heated at 35 ^{o}C and stirred for 24h. The mixture was then treated in an autoclave at 140 ^{o}C for 24h. The product was centrifuged at 14,240 relative centrifugal force (RCF; g-force) for 20 min, washed with deionized water, and dried at 60 ^{o}C. Finally, the product was calcined in air at 500 ^{o}C for 3h to remove the surfactant, and pure mesoporous silica KIT-6 was obtained.

2.4. Modification of KIT-6 with 3-mercaptopropyl-trimethoxysilane

Silane coupling agent was used as a surface modifier for KIT-6 by the following procedure: KIT-6 was dried at 105 °C for 3 h to remove the absorbed water. 40μL of 3-mercaptopropyl-trimethoxysilane and 0.4 g of KIT-6 were added into 25 mL of ethanol. They were mixed at room temperature under stirring, refluxed for 24 h, and then subjected to ultrasonic irradiation for 2 h. Finally, the suspension was collected by centrifuge (3560 RCF) and washed 3 times with 10 mL ethanol to remove unreacted silane coupling agent and then dried at 60 ^{o}C for 24 h to obtain modified KIT-6 (m-KIT-6).

2.5. In-situ synthesis of mesoporous silica nanocomposites (MSNCs)

MSNCs with m-KIT-6 contents of 1, 2, and 3 wt.% which was denoted as MSNC1%, MSNC2%, MSNC3%, respectively, were prepared using an *in-situ* method. For preparation of MSNCs, different amount of m-KIT-6 were added to 10 mL of dry toluene and sonicated in an ultrasonic bath for 1 h. Then MMA was added to the solution of the m-KIT-6 and the mixture was stirring to obtain a stable suspension and sonicated for 1 h. The BP initiator (1 wt.%) was added into the above solution and it was refluxed for 6 h. Polymerization was carried out under isothermal conditions. The solution was then poured into a clean glass, and the solvent was evaporated under a nitrogen atmosphere to formed PMMA and m-KIT-6 hybrids.

2.6. Adsorption studies: copper removal over pure KIT-6, m-KIT-6 and MSNCs

An essential parameter of heavy metal adsorption from wastewater, determining whether or not the use of a given sorbent is possible for approaching to an economical way is the contact time. So it is obvious the time it needs to reach the maximum capacity for capturing the hazardous material that needs to be separated, is an important investigation for heavy metal adsorption researches. In this study, the adsorption behavior of Cu(II) from aqueous solution by the MSNCs as well as pure KIT-6 and m-KIT-6 was investigated and kinetic and isotherm parameters were assessed. A stock solution of 1000 mg L^{-1} Cu(II) was prepared by dissolving

an weighed amount of analytical grade $Cu(NO_3)_2.3H_2O$ (>99.0% purity) in deionized water, the other solutions were prepared by dilution. Samples (10 mg) of the three types of MSNCs, pure KIT-6 and m-KIT-6 were added into 10 mL of 10 mg L^{-1} Cu(II) solution in a plastic container. The pH of the solution was adjusted to 5.5 with 1 M HCl and 0.1 M NaOH. The containers were placed in a shaker at a speed of 150 rpm and the contact time was varied from 1 to 255 min until the equilibrium was reached. The adsorbent was separated by centrifugation (3560 RCF, 10 min) and filtered through a 0.45 μm filter membrane. The residual Cu(II) concentrations were detected by flame atomic absorption spectrometer. The percentage of removed metal ions in the solution was computed using the following equation:

$$\%\ Removal = \frac{C_i - C_e}{C_i} \times 100 \quad (1)$$

Where C_i and C_e refer to the initial and equilibrium concentrations (mg L^{-1}) of Cu(II) in metal solution, respectively.

3. Results and discussion

3.1. Preparation of PMMA/mKIT-6 NCs

Scheme 1 shows the overall strategy applied for the preparation of MSNCs by the *in situ* synthesis approach. Possibly the most remarkable feature of ordered mesoporous KIT-6 is its ability to link with other active sites of molecules due to abundant active hydroxyl groups on the interior and exterior surface of its 3D framework. In addition to exterior surface modification of KIT-6, the penetration of silane coupling agents into the 3D interconnected pores of the KIT-6 and the interior surface modification provided a high active surface area with accessible functional groups for the following steps. MMA can be easily permeated into the 3D pores of m-KIT-6. So, before the start of the polymerization in the presence of initiator, monomers are present in and out of the 3D pores of m-KIT-6. Accordingly, it is possible that polymerization take place after adding initiator in both inside and outside of the pores. The interaction between carbonyl groups of polymer moiety and -OH and/or -SH on

the surface of modified mesoporous silica moiety during polymerization procedure lead to the formation of polymer chains through the 3D interconnected network of KIT-6. Hence, the advantage of this polymerization method compared to other methods is the higher percent polymerization into the interior pore space.

Scheme 1

3.2. Characterization techniques

3.2.1. FT-IR study

Fig. 1 shows the FT-IR spectra of pristine KIT-6 and silane modified KIT-6 (m-KIT-6). For neat KIT-6, a broad peak at 3200-3600 cm^{-1} was attributed to the O-H stretching of the silanol groups of the surface and the remaining adsorbed water molecules, while the peak at 1600-1630 cm^{-1} corresponds to bending mode of O-H of water. A broad and strong observed band between 1100 and 1250 cm^{-1}, corresponds to the siloxane groups (Si-O-Si), and the stretching band of the Si-O bonds at 806 cm^{-1} also recorded. In the FT-IR spectrum of the m-KIT-6, characteristic bands corresponding to the organic part of the silane coupling agent attached to the m-KIT-6, appearing at 2952 and 2894 cm^{-1} which were assigned to the C-H stretching vibration of the CH_2 of the propyl group and the band at 1470 cm^{-1} was assigned to the bending vibration of the C-H. This spectrum also showed peak at 2552 cm^{-1} that were characteristic of the SH of the coupling agent (Fig. 1). Thus the above spectrum indicated the reaction of coupling agent with KIT-6.

Fig. 1

The FT-IR spectra recorded for the pure PMMA and composite samples are depicted in Fig. 2. For PMMA, the absorption bands around 2997 and 2951 cm^{-1} corresponded to C-H asymmetric stretching in CH_3 and CH_2, respectively. The vibrational band at 2842 cm^{-1} was owing to the C-H symmetric stretching in CH_3. The characteristic band corresponded to C=O stretching was observed at 1732 cm^{-1} for the pure PMMA. The vibrations due to the

deformation modes of CH_3 groups appeared at 1486, 1450 and 1388 cm^{-1}. Bands at 1245 and 1273 cm^{-1} corresponded to C-O stretching modes. As shown in PMMA/m-KIT-6 NCs (MSNCs) spectra, the band around 1732 cm^{-1} which corresponds to carbonyl bond of PMMA, is shifted to lower wave numbers (1718 cm^{-1}) (red shift). The band at 1193 cm^{-1} corresponded to CH_3 wagging and the two bands at 1145 cm^{-1} and 1058 cm^{-1} were due to the CH_3 twisting, respectively. The vibration modes due to C-C stretching appeared at 988 cm^{-1} and 965 cm^{-1}. The peaks at 912 cm^{-1} and 840 cm^{-1} were assigned to CH_2 rocking and the peak at 750 cm^{-1} was due to the C-O out of plan bending.[36] In the FT-IR spectra of the PMMA/m-KIT-6 NCs, there were some new multiple absorption bands persisting in the region 400-600 cm^{-1} as well as 1070 cm^{-1}, mainly from the Si-O bands of m-KIT-6. Overall, these results indicated that there was a good interaction between the m-KIT-6 and PMMA matrix. Moreover, the peak intensity of the carbonyl bond in the spectrum of MSNCs is lower than that of pure PMMA. This may be due to the interaction between the mercapto groups of modified KIT-6 and C=O groups of PMMA (Fig. 2). This means that the double bond CO stretches become weak by hydrogen bonding to hydroxyl and mercapto groups. Thus, it is confirmed that hydrogen bonding between mercapto groups of modified KIT-6 and PMMA molecules exist on the surface of mesoporous KIT-6. As a result, these analyses show the formation of the PMMA/m-KIT-6 NCs.

Fig. 2

3.2.2. X-ray diffraction

The low-angle XRD patterns of the unmodified KIT-6 and m-KIT-6 are shown in Fig. 3. The XRD patterns of these samples indicated sharp diffraction peak at around 2θ = 0.84-0.93^o and two weak reflections at 2θ =1.34 and 1.68^o. As shown in Fig. 3, they can be indexed as the (2 1 0), (2 2 0) and (4 2 0) reflections of a 3-D cubic structure with *Ia3d* space group symmetry, respectively.[37] The diffraction peaks shifted a little to lower 2θ angles and

decreased progressively in intensity by modifications, which indicates that the ordered mesoporous structures were actually affected by the introduction of the organic substrate. Also, the XRD patterns of PMMA/m-KIT-6 NCs with different m-KIT-6 (2 and 3 wt.%) are shown in Fig. 3. In the MCNC with 2% of m-KIT-6, the XRD peaks of the m-KIT-6 can still be observed in the hybrid material which confirmed that ordered structures of KIT-6 have little aggregation and it may be uniformly dispersed throughout the polymer matrix, but in the MSNC 3% the peak of the mKIT-6 was disappeared.

Fig. 3

3.2.3. Morphology (FE-SEM and TEM)

Figures 4a and 4b show the morphological information of the pristine KIT-6 and m-KIT-6, respectively. As shown in these Figures, after modification, the surface morphology of KIT-6 have a litter changes and it is smoother than pristine KIT-6. To investigate the dispersion of the m-KIT-6 within the polymer matrix, the surface morphology of the PMMA with m-KIT-6 contents of 1, 2 and 3 wt% was investigated by FE-SEM technique. The results show that mesoporous m-KIT-6 into the PMMA matrix (Fig. 4c-4e). For the 1 and 2 wt% NCs (Fig. 4c, 4d), the filler distribution is apparently homogeneous due to the good adhesion between the inorganic and organic phases. In addition, when the amount of mKIT-6 reached to 3 wt%, the agglomerated particles were observed (Fig. 4e).

Fig. 4

The morphology of modified mesoporous KIT-6 and the distribution of the m-KIT-6 nanoparticles in the PMMA matrix were studied by TEM observations. The typical TEM micrographs clearly show that the m-KIT-6 has a well ordered cubic *Ia3d* pore array structure with an alternative pore channels. Pore size is approximately 8 nm based on the TEM image (Fig. 5a and 5b). After polymerization of MMA in the presence of 2 wt.% of m-KIT-6, shrinkage of pore channels was observed in the mesoporus KIT-6. According to the TEM

images, MSNC with 2% of m-KIT-6 showed an indistinct edge and a less disordered mesoporous structure due to the chain entanglement of PMMA on the surface of the m-KIT-6 and some aggregation could also be observed in the TEM images of this compound (Fig. 5c and 5d).

Fig. 5

3.2.4. Thermal properties

The thermal behavior of pristine KIT-6 and m-KIT-6 are shown in Fig. 6. By comparison of the TGA thermograms of modified KIT-6 with unmodified one, the results provide an indication of how the organic modifier effects the decomposition of the mesoporous material. Unmodified KIT-6 had a very small weight loss, with only 2 wt % around 600 ^{o}C.[10,12] After the functionalization of KIT-6 with silane coupling agent, the number of decomposition stages was increased. The first decomposition stage owing to the removal of water or silane coupling agent that physically absorbed at the surface of the m-KIT-6 was occurred at 100-250 ^{o}C. The second stage weight loss is from 280-450 ^{o}C, which may be attributed to the decomposition of the silane coupling agent. These results indicated the successful functionalization of the KIT-6.

Fig. 6

In order to examine the thermal stability, thermal analyses were carried out on PMMA and NCs of PMMA with 1, 2 and 3 wt% of m-KIT-6. The TGA thermogram of the pure PMMA and the composites are illustrated in Fig. 7. The thermal stability of these nanocomposites is higher than that of pure PMMA; the TGA data showing the temperature at which 10% degradation occurs, $T_{0.1}$, the temperature at which 50% degradation occurs, $T_{0.5}$, and the amount of material which is not volatile at 800 ^{o}C, char, are shown in Table 1. The temperature at which 10% degradation occurs is a measure of the onset temperature of the degradation and this is increased for all MSNC materials. Likewise, the temperature at which

50% degradation occurs is some measure of thermal stability, and this is 40 ^{o}C higher for all three MSNCs. The initial step of the degradation was attributed to the presence of weak links in the polymer chain and occurs at temperatures in the range of 170-200 ^{o}C. The amount of this first step is decreased in the presence of the KIT-6 and it occurs at a higher temperature in the range of 200-250 ^{o}C. Another degradation step occurs at about 200-400 ^{o}C for pristine PMMA, and for NC materials with different amount of m-KIT-6 is around 320-500 ^{o}C (Fig. 7). Overall, the resulting MSNCs had better thermal stability, as compared to PMMA, due to the good thermal stability of the m-KIT-6. This improvement could be due to the good interaction between the polymer matrix and mesoporous materials as well as the inherently good thermal stability of the mesoporous KIT-6.

Fig. 7

Table 1

3.3. Adsorption equilibrium

The lack of biodegradability of heavy metals leads to accumulation of these materials in living organisms. Copper ions at doses higher than the allowed amounts are known as a toxic contaminant. The accumulation of Cu(II) in the organs of human body can cause serious problems such as liver, heart, kidney, pancreas damages and gastrointestinal disturbance.[38] An essential parameters of heavy metal adsorption from wastewater determining whether or not the use of a given sorbent is possible for approaching to an economical way is the contact time. So it is obvious the time it needs to reach the maximum capacity for capturing the hazardous material that needs to be separated is an important investigation for heavy metal adsorption researches. In this study, pure KIT-6, m-KIT-6 and MSNCs were used for the removed of Cu (II) from the aqueous solution. In the case of MSNCs the free hydroxyl and mercapto groups of modified KIT-6 and carbonyl groups

available on the polymer matrix provided a good platform for the absorption process (Scheme 2).

Scheme 2

3.3.1 The effect of contact time

Figs. 8a and b showed that the adsorption rate of Cu(II) ions by the pure KIT-6 and m-KIT-6 increase rapidly until the contact time reaches 15 and 30 min, respectively. Also, the adsorption rate of Cu(II) by the MSNCs increase continuously until the contact time reaches 60, 90 and 90 min for the MSNCs 1%, MSNCs 2% and MSNCs 3%, respectively, and leveled off, until the Cu(II) removal attained equilibrium, Beyond these limits has no considerable increasing in the removal percentage, suggesting that all the adsorption sites have been occupied. The fast adsorption of Cu(II) ions at the initial stages by three types of MSNCs, pure KIT-6 and m-KIT-6 can be interpreted by availability of the uncovered surface and active sites of mesoporous silica and NCs. Within 255 min of the contact time, the maximum adsorptive capacity of tree types of MSNCs 79.14 %, 91.20 % and 81.72 %, was attained, respectively. Also, the adsorption of two species adsorbent, pure and modified KIT-6, was higher than 97% through optimum time (Fig 8).

Fig. 8

3.3.2 *Adsorption kinetic*

The amounts of metal adsorbed per unit mass of adsorbent at equilibrium (q_e, mg g^{-1}) and at any time (q_t, mg g^{-1}) (adsorption capacity) were calculated according to:

$$q_e = (C_i - C_e)V/m \quad (2)$$

$$q_t = (C_i - C_t)V/m \quad (3)$$

where C_t (mg L^{-1}) is the metal concentrations at the equilibrium and at any time t, V(L) is the volume of the solution, and m (g) is the amount of sorbent. Sorbent performance was

frequently evaluated with the distribution coefficient (K_d) (in mLg^{-1}).[39] K_d was calculated according to Equation 4 and the results are summarized in Table 2:

$$K_d = [(C_i - C_e)/C_e] \times (V/m) \qquad (4)$$

The values of K_d for pure KIT-6, m-KIT-6 and MSNCs are shown in Fig 9.

Fig. 9

To investigate the changes in sorption with time and quantifying an appropriate mechanism of adsorption kinetic models, pseudo-second-order, Elovich, and intra-particle diffusion equations are used to interpret the experimental data.[40-42] The pseudo-second-order equation may be represented in a linear form as:

$$\frac{t}{q_t} = \frac{1}{\alpha} + \frac{1}{q_e} t \qquad (5)$$

$$and \quad \alpha = k_{ad} q_e^2 \qquad (6)$$

where α is the initial sorption rate ($mg\ g^{-1}\ min^{-1}$) and k_{ad} is the pseudo-second-order rate constant of adsorption ($g\ mg^{-1}\ min^{-1}$). The slope and intercept of the plot of t/q_t versus t are used to calculate k_{ad} and $q_{e,cal}$ (Fig. 10).

Elovich kinetic equation is generally expressed by the following equation:

$$q_t = \frac{\ln(\alpha\beta)}{\beta} + \frac{\ln t}{\beta} \qquad (7)$$

where β is the desorption constant ($mg\ g^{-1}\ min^{-1}$).

Intra-particle diffusion describes the movement of species from the bulk of the solution to the solid phase. It is given by Weber and Morris:

$$q_t = k_{intra}(t)^{1/2} + C \qquad (8)$$

Where k_{intra} is the intra-particle diffusion rate constant ($mg\ g^{-1}\ min^{-1}$), which may be taken as a rate factor and C is a constant. The intra-particle diffusion plots exhibited a multi-linear correlation which revealed that two or more steps occurred during the adsorption

process (Fig. 8c and d and Table 2). The first step, can be attributed to the external surface adsorption (intra-particle diffusion), and the second one is the pore diffusion.[43, 44]

Table 2

Fig. 10

The corresponding three kinetic parameters from these three models are illustrated in Table 3. According to the obtained results, it was found that pseudo second order equation provides larger correlation coefficient values than the Elovich model when using the pure KIT-6 and m-KIT-6 as sorbents. For MSNCs, the pseudo-second order model represented the better proximity of correlation coefficient values ($R_1^2 > 99\%$) than those of the Evolich (R_2^2) and intra-particle diffusion (R_3^2) models for three types of MSNCs. Also the calculated q_e values ($q_{e,cal}$) from pseudo-second-order model was close to the experimental q_e values ($q_{e,exp}$), suggesting that the chemical adsorption can be well described with the pseudo-second-order kinetic model for pure KIT-6, m-KIT-6 and MSNCs. These data expressed that the adsorption is very fast, probably controlled by chemical adsorption which might involve the valency forces through sharing or exchange of electrons between Cu(II) ions and adsorbents.[44, 45]

Table 3

3.3.3 Adsorption isotherm

Adsorption behavior and adsorption capacity of Cu(II) ions onto pure Kit-6, m-KIT-6 and MSNCs can be described by an adsorption isotherm (Fig. 11a). Aqueous solution of Cu(II) with different initial concentration were prepared for investigating of adsorption isotherm at a constant pH and optimum times at room temperature. Among different adsorption isotherm models we selected Lnagmuir [46] and Freundlich [47] models for describing adsorption behavior of Cu(II) ions which are widely used in experimental works. The Langmuir isotherm model is applied to describe the monolayer adsorption of an adsorbents

onto a structurally homogeneous surface with a finite number of identical sites. The adsorption process is completed when these identical sites are occupied by adsorbents. Mathematically, the linearized form of the Langmuir model can be written in the following form:

$$C_e/q_e=1/K_Lq_{max}+C_e/q_{max} \quad (9)$$

Where C_e is equilibrium concentration of the metal ions (mg/L) and q_e is the solid phase equilibrium concentration. Q_m is the maximum sorption capacity (mg/g), and K_L is a constant related to binding energy of the sorption system (L/mg). The K_L and q_m can be obtained from the intercept and slop of the linear plots when C_e/q_e results in a fairly straight line.

Unlike the Langmuir isotherm, the Freundlich isotherm model is derived to describe the multilayer adsorption of an adsorbate onto a heterogeneous surface of an adsorbent. The linear form of Freundlich isotherm model can be represented by logarithmic Eq.(10):

$$\text{Log } q_e = \log K_f + 1/n.\ \log C_e \quad (10)$$

Where n and K_f are the Freundlich isotherm constant. K_f $(mg/g)(mg/L)^{1/}n$ and n relate to the adsorption capacity and intensity of a given adsorbent, respectively.

The values of the constants in both models are obtained from the slope and the position (Fig. 11b and c). Table 4 shows the results of the fit and of the constants of both models for three adsorbents including pure KIT-6, m-KIT-6 and MSNCs 2%. The values of n for pure KIT-6, m-KIT-6 and MSNCs 2% were 1.33, 1.29 and 1.95, respectively. The values between 1-10 for n in the adsorption process are favorable according to Slejko.[48] All the correlation coefficients and parameters obtained for the isotherm models from Table 4 reveal that the Langmuir isotherm is the best model to demonstrate the adsorption of Cu(II) onto pure KIT-6, m-KIT-6 and MSNCs.

Table 4

Fig. 11

4. Conclusions

Novel mesoporous silica nanocomposites (MSNCs) were prepared by *in situ* polymerization of MMA and modified KIT-6 as filler. The m-KIT-6 was prepared through the reaction between 3-mercaptopropyl-trimethoxysilane with hydroxyl groups of the surface mesoporous KIT-6. The chemical, structural and textural properties of MSNCs were characterized by several methods. Due to the good interaction between the polymer matrix and mesoporous KIT-6 as well as the inherently good thermal stability of the mesoporous KIT-6, TGA results show an improvement in the thermal properties of the MSNCs in comparisons to the neat PMMA. Then, the application of the MSNCs for adsorption of Cu(II) from aqueous solution was examined. As a comparison between three types of MSNCs, it can easily observed that MSNCs 2% exhibit higher adsorption capacities that other MSNC1% and MSNC2%. In addition Higher k_d values representing more effecting sorbents for removal of heavy metals and so MSNC2% have a more effective adsorption capacity in comparisons to MSNC1% and MSNC3%. Also, it was observed the time necessary for the MSNCs reach the equilibrium is short (60-90 min), when compared to the other sorbents, which in general conditions only achieve equilibrium state after several hours of exposure. In addition, the equilibrium data for Cu(II) ions confirm that Langmuir isotherm is the best model for interpreting adsorption mechanism according to R^2 values of four adsorbents.

Acknowledgments

This work was partially funded by the Research Affairs Division of Isfahan University of Technology (IUT) and Iran Nanotechnology Initiative Council (INIC).

Notes

The authors declare no competing financial interest.

References

1. U. Ciesla and F. Schüth, *Microporous and Mesoporous Materials*, 1999, **27**, 131-149.
2. C. Liu, F. Li, L.-P. Ma and H.-M. Cheng, *Adv. Mater.*, 2010, **22**, E28-E62.
3. M. Vallet-Regí, F. Balas and D. Arcos, *Angewandte Chemie International Edition*, 2007, **46**, 7548-7558.
4. M. Hartmann, *Chemistry of Materials*, 2005, **17**, 4577-4593.
5. Z. Wu and D. Zhao, *Chemical Communications*, 2011, **47**, 3332.
6. M. Dinari, G. Mohammadnezhad, A. Nabiyan, Colloid and Polymer Science 2015, **293**, 1569-1575.
7. M. Laghaei, M. Sadeghi, B. Ghalei, M. Dinari. Progress in Organic Coatings 2016, **90**, 163-170.
8. H. Zou, S. Wu and J. Shen, *Chemical Reviews*, 2008, **108**, 3893-3957.
9. I. A. Rahman and V. Padavettan, *Journal of Nanomaterials*, 2012, **2012**, 1-15.
10. J. Wang, Y. Li, Z. Zhang and Z. Hao, *J. Mater. Chem. A*, 2015, **3**, 8650-8658.
11. J. KukáShon, S. SungáKong, J. ManáKim, C. HyunáKo, Y. YunáLee, S. HeeáHwang and J. AháYoon, *Chemical Communications*, 2009, 650-652.
12. M. Dinari, G. Mohammadnezhad and A. Nabiyan, *Journal of Applied Polymer Science*, 2016, **133,** 43098-43103.
13. K. Soni, B. S. Rana, A. K. Sinha, A. Bhaumik, M. Nandi, M. Kumar and G. M. Dhar, *Applied Catalysis B: Environmental*, 2009, **90**, 55-63.
14. R. J. Kalbasi and N. Mosaddegh, *Journal of Inorganic and Organometallic Polymers and Materials*, 2012, **22**, 404-414.
15. R. Kishor and A. K. Ghoshal, *Chemical Engineering Journal*, 2015, **262**, 882-890.
16. H. Zhao, S. Liu, R. Wang and T. Zhang, *Materials Letters*, 2015, **147**, 54-57.
17. F. Li, N. van der Laak, S.-W. Ting and K.-Y. Chan, *Electrochimica Acta*, 2010, **55**, 2817-2823.
18. D. Zhang, L. Zheng, Y. Ma, L. Lei, Q. Li, Y. Li, H. Luo, H. Feng and Y. Hao, *ACS Appl. Mater. Interfaces*, 2014, **6**, 2657-2665.
19. L. Ma'mani, S. Nikzad, H. Kheiri-manjili, S. al-Musawi, M. Saeedi, S. Askarlou, A. Foroumadi and A. Shafiee, *European Journal of Medicinal Chemistry*, 2014, **83**, 646-654.
20. J. Ceballos-Torres, P. Virag, M. Cenariu, S. Prashar, M. Fajardo, E. Fischer-Fodor and S. Gómez-Ruiz, *Chemistry - A European Journal*, 2014, **20**, 10811-10828.
21. W. Sun, L. Li, E. A. Stefanescu, M. R. Kessler and N. Bowler, *Journal of Non-Crystalline Solids*, 2015, **410**, 43-50.
22. J. Hong, S. Lee, J. Seo, S. Pyo, J. Kim and T. Lee, *ACS Appl. Mater. Interfaces*, 2015, DOI: 10.1021/am5073645, 150209062057005.
23. Z. Fan, F. Gong, S. T. Nguyen and H. M. Duong, *Carbon*, 2015, **81**, 396-404.
24. W. F. Mousa, M. Kobayashi, S. Shinzato, M. Kamimura, M. Neo, S. Yoshihara and T. Nakamura, *Biomaterials*, 2000, **21**, 2137-2146.
25. N. B. Trung, T. V. Tam, D. K. Dang, K. F. Babu, E. J. Kim, J. Kim and W. M. Choi, *Chemical Engineering Journal*, 2015, **264**, 603-609.
26. V. M. Cuijpers, J. Jaroszewicz, S. Anil, A. Al Farraj Aldosari, X. F. Walboomers and J. A. Jansen, *Clinical oral implants research*, 2014, **25**, 359-365.
27. S. Kango, S. Kalia, A. Celli, J. Njuguna, Y. Habibi and R. Kumar, *Progress in Polymer Science*, 2013, **38**, 1232-1261.
28. G. Mohammadnezhad, M. Dinari, R. Soltani and Z. Bozorgmehr, *Applied Surface Science*, 2015, **346**, 182-188.
29. J. Jiao, l. Wang, P. Lv, P. Liu and Y. Cai, *Materials Letters*, 2013, **109**, 158-162.
30. J.-X. Yu, L.-Y. Wang, R.-A. Chi, Y.-F. Zhang, Z.-G. Xu and J. Guo, *Applied Surface Science*, 2013, **268**, 163-170.

31. A. R. Keshtkar, M. Irani and M. A. Moosavian, *Journal of the Taiwan Institute of Chemical Engineers*, 2013, **44**, 279-286.
32. S. Egodawatte, A. Datt, E. A. Burns and S. C. Larsen, *Langmuir*, 2015, **31**, 7553-7562.
33. L. Wang, C. Cheng, S. Tapas, J. Lei, M. Matsuoka, J. Zhang and F. Zhang, *J. Mater. Chem. A*, 2015, **3**, 13357-13364.
34. B. Samiey, C.-H. Cheng and J. Wu, *Materials*, 2014, **7**, 673-726.
35. L. Qian, Y. Ren, T. Liu, D. Pan, H. Wang and G. Chen, *Chemical Engineering Journal*, 2012, **213**, 186-194.
36. Z. Jia, Z. Wang, C. Xu, J. Liang, B. Wei, D. Wu and S. Zhu, *Materials Science and Engineering: A*, 1999, **271**, 395-400.
37. A. Ramanathan, B. Subramaniam, D. Badloe, U. Hanefeld and R. Maheswari, *Journal of Porous Materials*, 2012, **19**, 961-968.
38. T. Aman, A. A. Kazi, M. U. Sabri and Q. Bano, *Colloids and Surfaces B: Biointerfaces*, 2008, **63**, 116-121.
39. W. Yantasee, C. L. Warner, T. Sangvanich, R. S. Addleman, T. G. Carter, R. J. Wiacek, G. E. Fryxell, C. Timchalk and M. G. Warner, *Environmental Science & Technology*, 2007, **41**, 5114-5119.
40. B. M. W. P. K. Amarasinghe and R. A. Williams, *Chemical Engineering Journal*, 2007, **132**, 299-309.
41. S. Chien and W. Clayton, *Soil Science Society of America Journal*, 1980, **44**, 265-268.
42. C. Namasivayam and K. Ranganathan, *Water Research*, 1995, **29**, 1737-1744.
43. T. A. Saleh, *Desalination and Water Treatment*, 2015, 1-15.
44. Q. Yuan, Y. Chi, N. Yu, Y. Zhao, W. Yan, X. Li and B. Dong, *Materials Research Bulletin*, 2014, **49**, 279-284.
45. S. Wang, K. Wang, C. Dai, H. Shi and J. Li, *Chemical Engineering Journal*, 2015, **262**, 897-903.
46. I. Langmuir, *Journal of the American Chemical society*, 1918, **40**, 1361-1403.
47. H. Freundlich, *J. Phys. Chem*, 1906, **57**, e470.
48. F. L. Slejko, *Adsorption technology. A step-by-step approach to process evaluation and application*, Dekker New York; Basel, 1985.

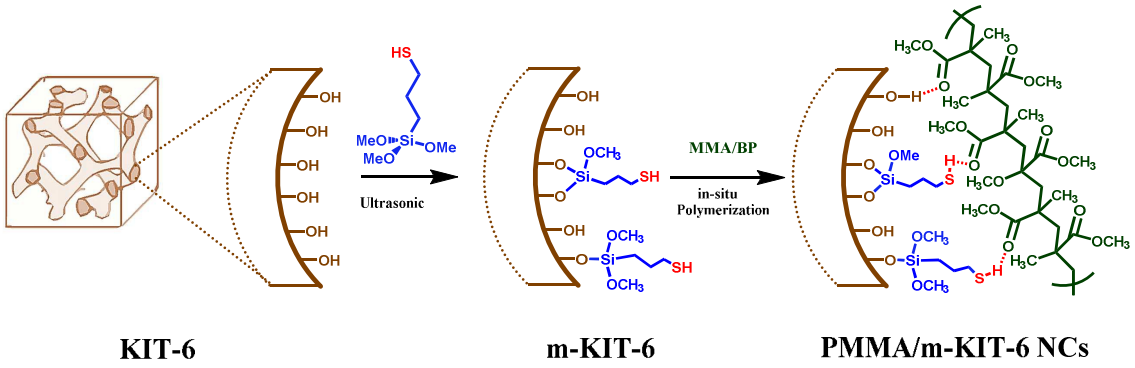

KIT-6 **m-KIT-6** **PMMA/m-KIT-6 NCs**

Scheme 1. Surface modification of mesoprous KIT-6 and preparation of PMMA/mKIT-6 hybrid materials.

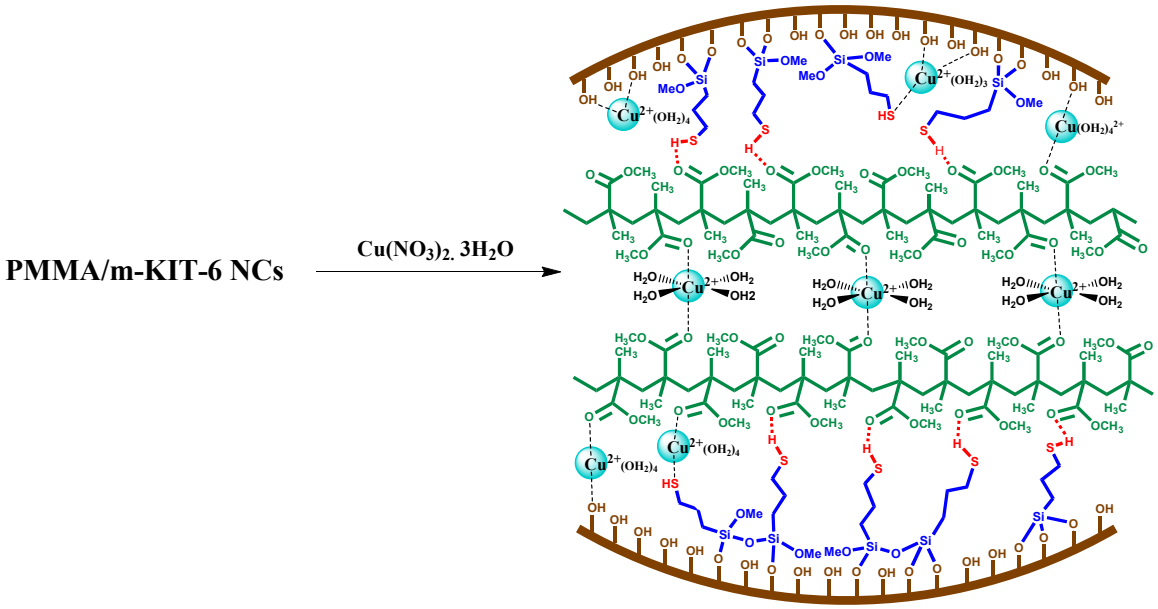

Scheme 2. Adsorption of Cu^{2+} by MMA/mKIT-6 hybrid materials

Table 1. Thermal properties of the PMMA and NC with different amount of m-KIT-6.

Samples	Decomposition temperature (^oC)		Char (%)[c]
	$T_{0.1}$ (^oC)[a]	$T_{0.5}$ (^oC)[b]	
PMMA	186	367	2
MSNC1%	315	401	5
MSNC2%	332	428	7
MSNC3%	345	456	8

[a] Temperature at which 10% degradation occurs. [b] Temperature at which 50% degradation occurs. [c] The amount of material which is not volatile at 800 ^oC.

Table 2. adsorption quality and distribution coefficient parameters for Cu(II) solution (10 mg L^{-1}, pH=5.5) on three types of MSNCs.

Sorbent	Content solution (mg/L)		Removal efficiency %	Cu(II) adsorbed on sorbent		k_d
	Initial (C_i)	Final (C_e)		(mg/g)	(μ mol/g)	(mL/g)
Pure KIT-6	10	0.19	98.08	9.81	154.37	51.63×10^3
m-KIT-6	10	0.10	99.00	9.90	155.80	99.00×10^3
MSNCs 1%	10	2.26	77.41	7.74	121.80	3.42×10^3
MSNCs 2%	10	0.96	90.34	9.03	142.10	9.42×10^3
MSNCs 3%	10	1.83	81.72	8.17	128.57	4.46×10^3

Table 3. Comparison of the kinetic parameters for three types of MSNCs in Cu(II) adsorption.

Sorbent	$q_{e,exp}$ (mg/g)	α (mg/g min)	Pseudo second order			Elovich kinetic		Intra-particle diffusion		
			$q_{e,cal}$ (mg/g)	k_{ad} (g/mg min) $\times 10^{-3}$	R^2_1	β (mg/g min)	R^2_2	k_{intra} (mg/g min)	C	R^2_3
Pure KIT-6	9.81	9.75	9.99	97.69	0.9993	0.809	0.8108	0.6791	6.3136	0.6139
m-KIT-6	9.90	16.79	9.96	169.25	0.9998	1.372	0.8935	0.4155	7.6994	0.7285
MSNCs 1%	7.74	1.12	8.26	16.38	0.9978	0.886	0.7272	0.2132	5.1630	0.5423
MSNCs 2%	9.03	1.23	9.47	13.73	0.9992	0.894	0.8440	0.2200	6.1779	0.6817
MSNCs 3%	8.17	0.91	8.60	12.31	0.9980	0.812	0.8021	0.2392	5.0329	0.6323

Table 4. Adsorption equilibrium constant for Langmuir and Freudnlich isotherm equation

Sorbents	Langmuir isotherm equation			Freundlich isotherm equation		
	$q_{max}(mg/g)$	$K_L(L/mg)$	R^2	$K_f(mg/g)$	$1/n$	R^2
Pure KIT-6	76.92	0.163	0.9987	9.497	0.7492	0.9860
m-KIT-6	102.04	0.134	0.9989	10.824	0.7774	0.9874
MSNCs 2%	24.45	0.583	0.9990	6.977	0.5134	0.9489

Legends for Figures

Fig. 1. FT-IR spectra of the pure KIT-6 and mKIT-6.

Fig. 2 FT-IR spectra of the neat PMMA and NCs of PMMA with different amount of m-KIT-6.

Fig. 3 XRD patterns of the KIT-6, m-KIT-6, and NC of PMMA with 2 and 3 wt.% of m-KIT-6.

Fig. 4 FE-SEM images of pristine KIT-6 (a), m-KIT-6 (b) and NCs of PMMA with 1 (c), 2 (d) and 3 wt.% (e) of m-KIT-6.

Fig. 5 TEM images of m-KIT-6 (a, b) and MSNC with 2 wt.% of m-KIT-6 (c, d).

Fig. 6 TGA thermograms of the KIT-6 (a) and m-KIT-6 (b).

Fig. 7 TGA thermograms of the PMMA and NCs of PMMA with different amount of m-KIT-6.

Fig. 8. The effect of contact time on Cu(II) adsorption by pure KIT-6, m-KIT-6 (a) and MSNCs with different m-KIT (b) (Contact time = 255 min, pH = 5.5, agitation speed = 150 rpm, initial Cu(II) concentration = 10 mg L^{-1}, and adsorbent dosage = 10 mg), intra-particle diffusion plot for the removal of Cu(II) by pure KIT-6, m-KIT-6 (c) and MSNCs with different m-KIT (d).

Fig. 9. Distribution coefficient (K_d) of pure KIT-6, m-KIT-6 and MSNCs with different m-KIT.

Fig. 10. Pseudo-second-order kinetics plots for the adsorption of Cu (II).

Fig. 11. Isotherm equilibrium (a), Langmuir plot for Cu(II) on the pure KIT-6, m-KIT-6 and MSNCs, pH=5.5 (b) Freundlich plot for Cu(II) on the pure KIT-6, m-KIT-6 and MSNCs, pH=5.5 (c).

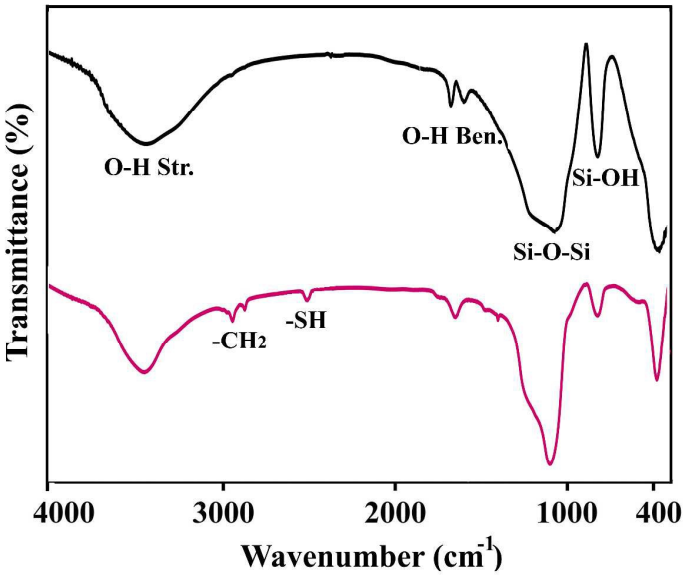

Fig. 1. FT-IR spectra of the pure KIT-6 and mKIT-6.

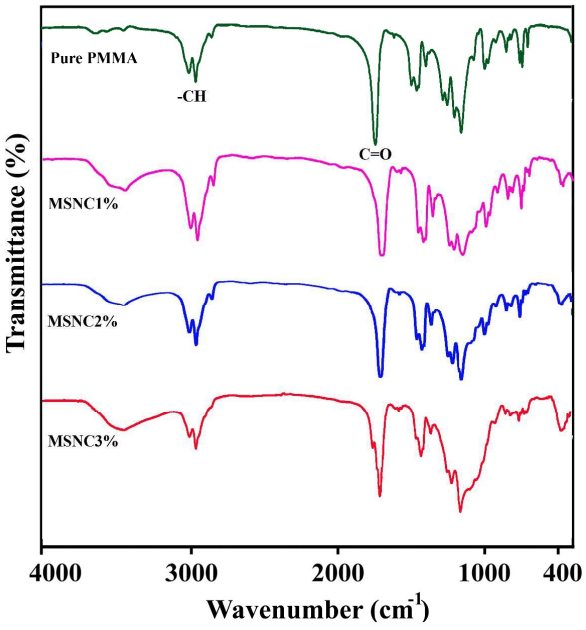

Fig. 2

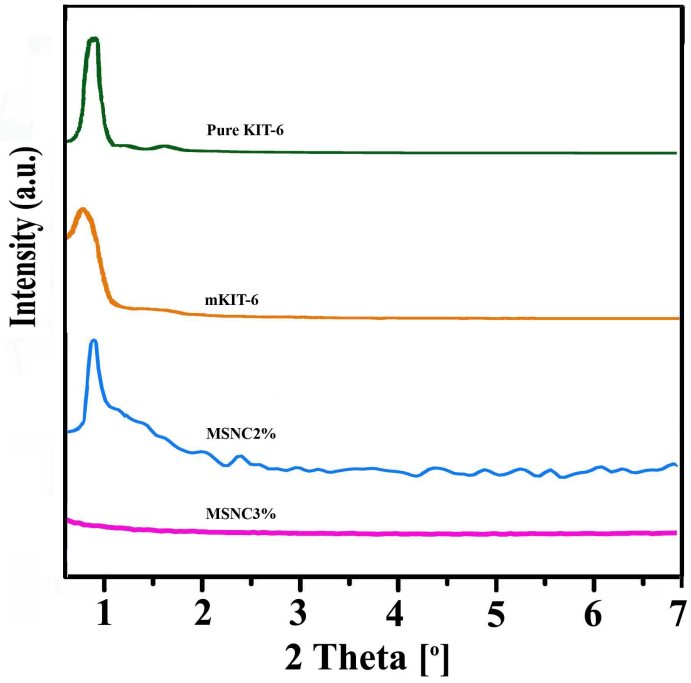

Fig. 3

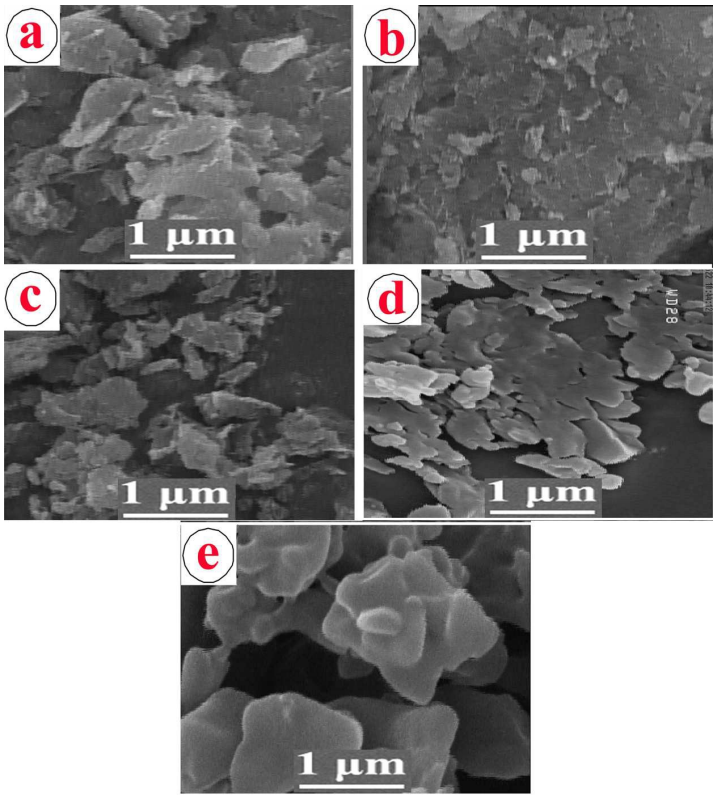

Fig. 4

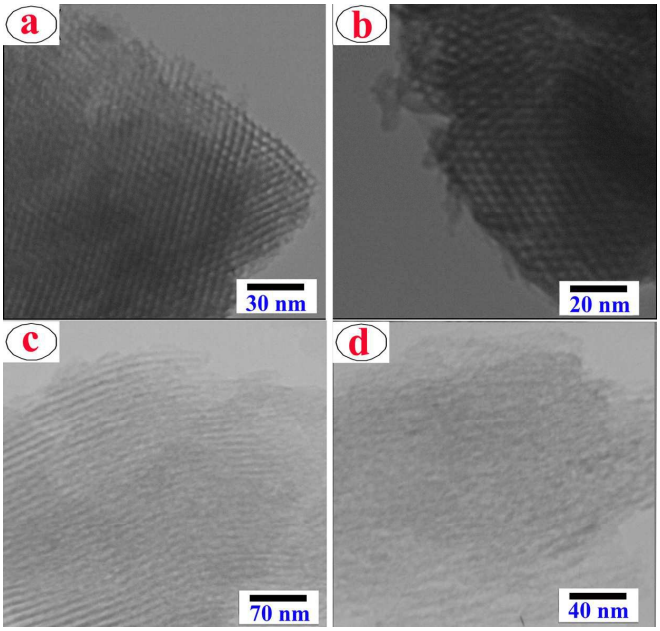

Fig. 5

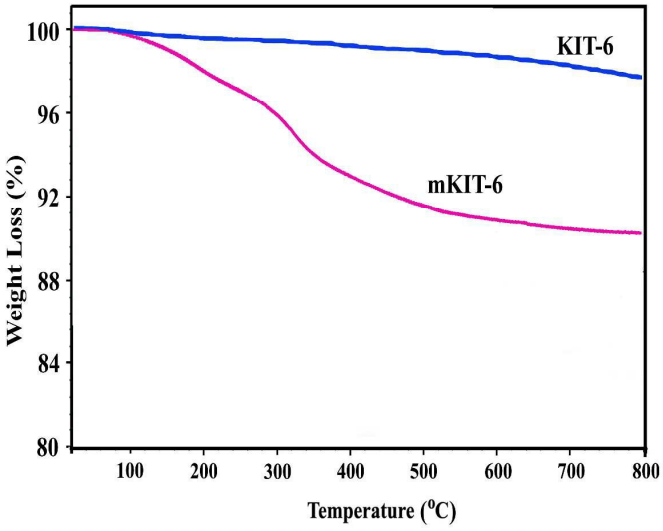

Fig. 6

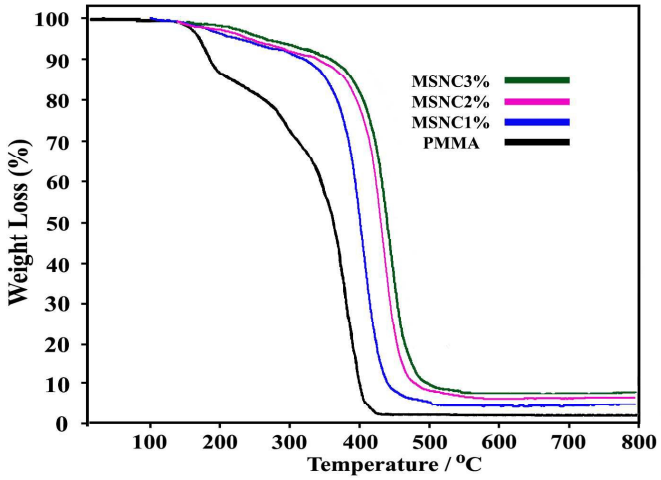

Fig. 7

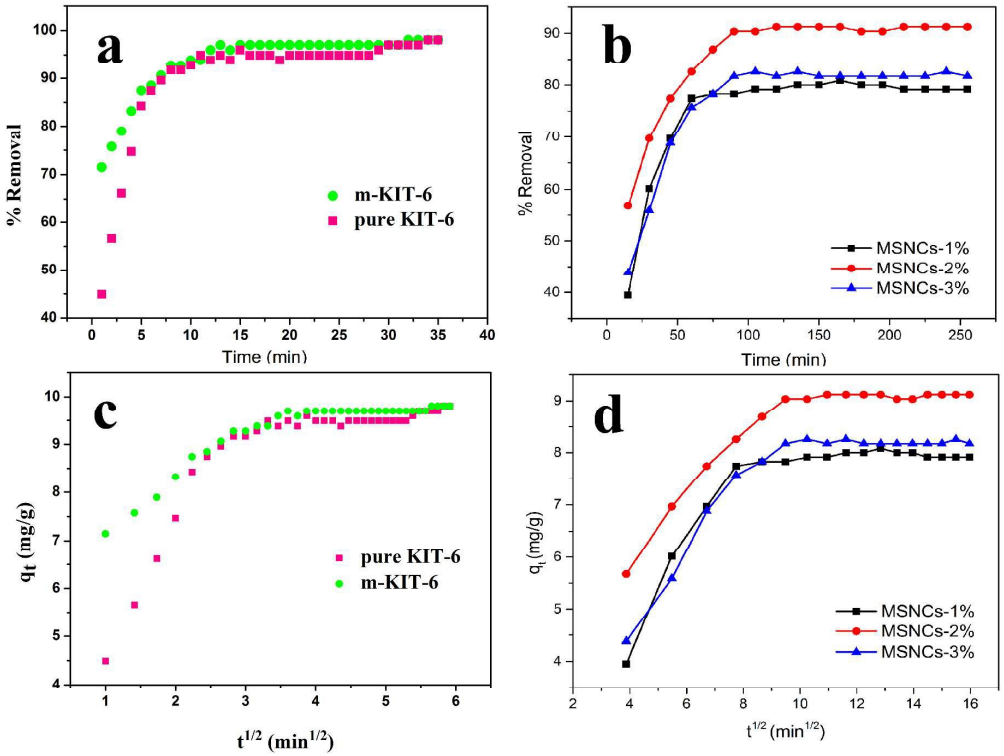

Fig. 8

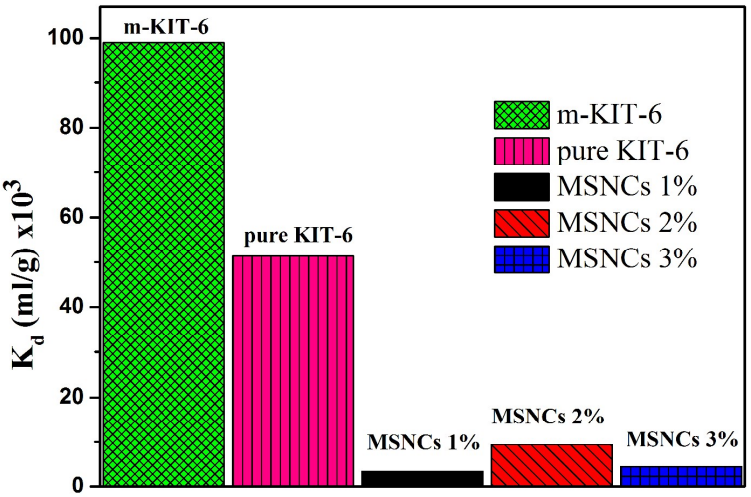

Fig. 9

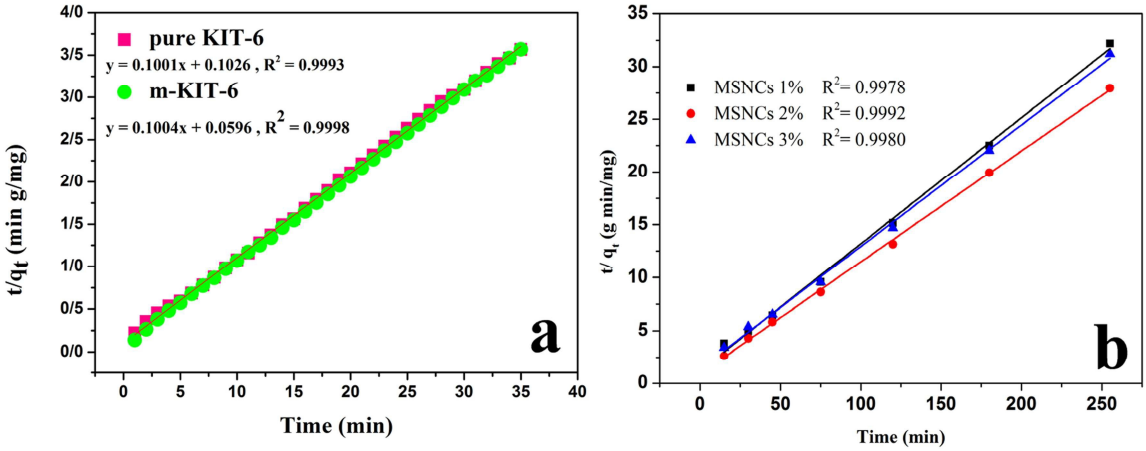

Fig. 10

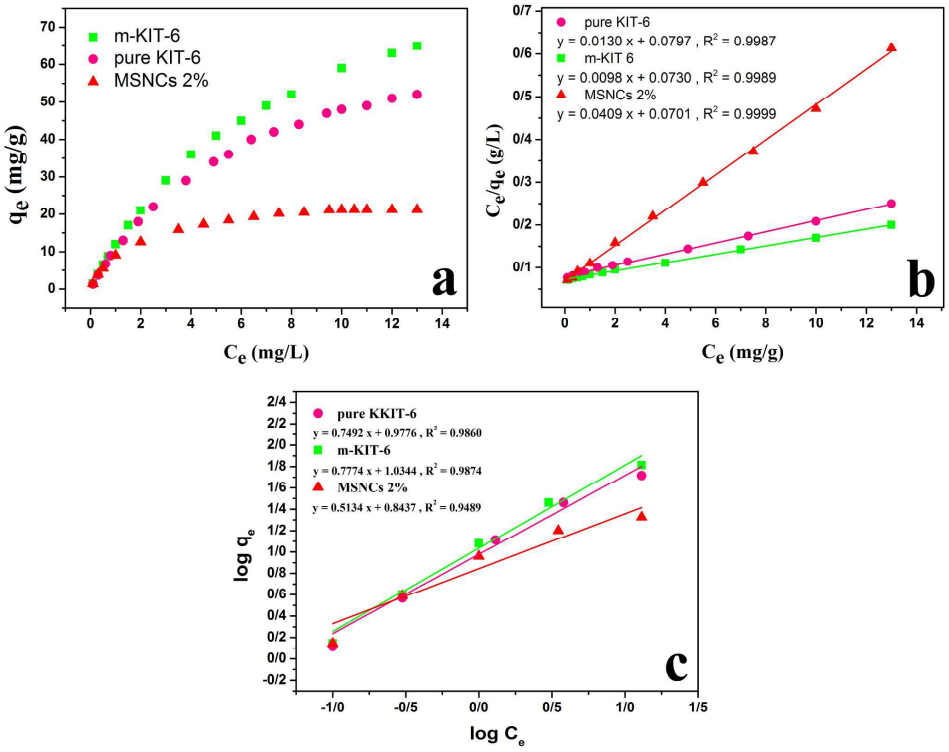

Fig. 11

Novel mesoporous silica nanocomposites for adsorption of Cu(II) from aqueous solution were prepared by *in situ* polymerization of MMA and modified KIT-6 as filler.